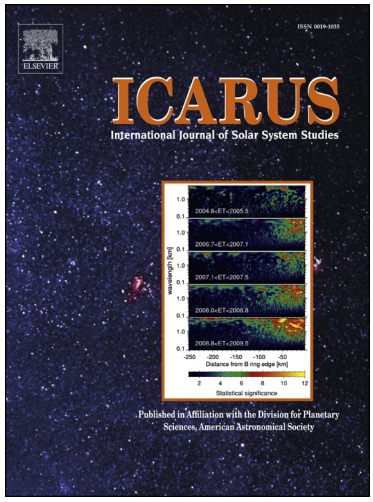

On the chemical composition of Titan's dry lakebed evaporites

D. Cordier, J.W. Barnes, A.G. Ferreira

PII: S0019-1035(13)00327-8
DOI: http://dx.doi.org/10.1016/j.icarus.2013.07.026
Reference: YICAR 10737

To appear in: *Icarus*

Received Date: 10 March 2013
Revised Date: 15 July 2013
Accepted Date: 22 July 2013

Please cite this article as: Cordier, D., Barnes, J.W., Ferreira, A.G., On the chemical composition of Titan's dry lakebed evaporites, *Icarus* (2013), doi: http://dx.doi.org/10.1016/j.icarus.2013.07.026

On the chemical composition of Titan's dry lakebed evaporites

D. Cordier[a], J. W. Barnes[b], A. G. Ferreira[c]

[a] *Université de Franche-Comté, Institut UTINAM, CNRS/INSU, UMR 6213, 25030 Besançon Cedex, France*
[b] *Department of Physics, University of Idaho, Engineering-Physics Building, Moscow, ID 83844, USA*
[c] *Departamento de Engenharia Quimica, Universidade de Coimbra, Coimbra 3030-290, Portugal*

Abstract

Titan, the main satellite of Saturn, has an active cycle of methane in its troposphere. Among other evidence for a mechanism of evaporation at work on the ground, dry lakebeds have been discovered. Recent *Cassini* infrared observations of these empty lakes have revealed a surface composition poor in water ice compared to that of the surrounding terrains — suggesting the existence of organic evaporites deposits. The chemical composition of these possible evaporites is unknown. In this paper, we study evaporite composition using a model that treats both organic solids dissolution and solvent evaporation. Our results suggest the possibility of large abundances of butane and acetylene in the lake evaporites. However, due to uncertainties of the employed theory, these determinations have to be confirmed by laboratory experiments.

Keywords: planets and satellites: individual: Titan – planets and satellites: general – solar system: general

1. Introduction

For a long time the existence of liquid hydrocarbons at the surface of Titan has been suspected (Sagan and Dermott, 1982; Lunine et al., 1983; Lunine, 1993a,b). The dark features observed by Stofan et al. (2007) in the

Email address: daniel.cordier@obs-besancon.fr (D. Cordier)

north polar region were the first confirmed lakes or seas of hydrocarbons. Subsequently, other evidence for the RADAR-dark areas' lacustrine nature was found in the RADAR and IR ranges, to the extent that the existence of lakes/seas is now rather well established. In fact, the number of detected manifestations (e.g. Turtle et al., 2011a,b) of an active tropospheric methane hydrologic cycle is increasing. The lakes are expected to take part in this cycle, providing methane and/or ethane to the atmosphere through evaporation processes.

In past years, the signature of lake evaporation has been actively researched. Already, Stofan et al. (2007) noticed features showing margins similar to those of established lakes but having a RADAR surface backscatter similar to the surrounding terrain, suggesting the occurrence of an evaporation process in the recent past. Barnes et al. (2009) performed a detailed study of shoreline features of Ontario Lacus, the largest southern latitude lake. These authors interpreted the 5-μm bright annulus around Ontario Lacus as a dry, low-water ice content zone, possibly corresponding to a deposit of fine-grained organic condensates. These patterns, created by the shoreline recession, could have been caused by an evaporation episode. In their study of the same system, Wall et al. (2010) reported evidences for active shoreline processes. Although evidence for short-term changes in the extent of Ontario Lacus has been put forward (Turtle et al., 2011b), a subsequent reanalysis came to the conclusion that there is no indication of lake extent changes in the *Cassini* dataset (Cornet et al., 2012). Hayes et al. (2011) noticed that some observed dry lakebeds in Titan's arctic appear to be brighter than their exteriors in both nadir and off-nadir observations, which suggests compositional differences. However Hayes et al. (2011) were not able to exclude the possibility of an infiltration of liquids into a subsurface hydrologic system. Barnes et al. (2011a) used a sample of several lakes and lakebeds located in a region south of the Ligeia Mare. They obtained a strong correlation between RADAR-empty lakes and 5-μm-bright unit interpreted as low-water ice content areas.

As mentioned by Barnes et al. (2011a) these observed dry lake floors cannot be made only of sediments, indeed a pure sedimentary origin of these deposits would produce lakebed showing a 5-μm-brightness similar to that of their surrounding zones. One possible explanation proposed by Barnes et al. (2011a) consists of evaporation of the solvent (here a mixture of methane and ethane) yielding to the saturation of the dissolved solutes. The top layer of the resulting evaporites is being observed now in dry lakebeds if this idea

is correct. This paper is devoted to an exploration of the evaporite scenario on the theoretical side. We have developed a model allowing for the computation of the chemical composition of such evaporites.
This paper is organized as follows. In Sect. 2, we outline our model for calculating chemical composition of putative evaporite deposits in dry lakebeds. Sect. 3 is devoted to evaporite composition computations, and we discuss our results and conclude in Sect. 4.

2. Model Description

We consider a portion of a Titan lake of uniform depth h that has a free surface of area S in contact with the atmosphere. For the sake of simplicity, methane, ethane and nitrogen are considered to be the only volatile compounds; they form a ternary mixture which will be our solvent. The presence of H_2, Ar and CO is neglected as they have low abundances in the atmosphere and as a consequence in the solution; C_3H_8 and C_4H_8 are also not taken into account because C_2H_6 seems to be much more abundant and their behaviors should not be very different than that of ethane. In addition to the solvent chemistry itself, we considered species in the solid state under Titan's surface thermodynamic conditions that may dissolve in the solvent. In the following, for short, we will simply call these compounds "dissolved solids" or "solutes": they include all the species, except those belonging to the solvent (*i.e.*, methane, ethane and nitrogen). These supposed dissolved species are ultimately the products of the complex photochemistry taking place in the upper Titan atmosphere. In this work, we used the same list of solid compounds as in previous papers (Cordier et al., 2009, 2010, 2012, hereafter respectively C09, C10 and C12. Note that Cordier et al. (2013) is an erratum of Cordier et al. (2009).) These species appear to be among the main products found by photochemical 1D-models of Lavvas et al. (2008a,b) and Vuitton et al. (2008); the list is displayed in Table 1. This list differs from the list of species detected by CIRS[1] (*i.e.*, CH_4, C_2H_2, C_2H_4, C_2H_6, C_3H_8, CH_3C_2H, C_4H_2, C_6H_6, HCN, HC_3N, C_2N_2, CO, CO_2 and H_2O, see Vinatier et al., 2010) as CIRS observations relate to Titan's stratosphere and do not imply that these species reach the thermodynamic conditions of their precipitation to the ground. In addition, some species (for instance

[1]Composite Infrared Spectrometer, an instrument onboard the Cassini spacecraft.

C_4H_3, C_4H_4, C_4H_5; see Tab. 5 of Lavvas et al., 2008a) are included in models while they are not yet observed by Cassini instruments. Thanks to their melting temperatures ranging between 136.0 K (C_4H_{10}) and 279.1 K (C_6H_6), all these molecules are in solid state under the Titan's surface conditions ($T \sim 90$ K in the region of lakes; Jennings et al., 2009). Although it has still to be confirmed by laboratory experiments, the materials listed in Table 1 are theoretically predicted to be soluble in a mixture of methane and ethane. Indeed, the Hildebrand's solubility parameters δ's for these solids (see Poling et al., 2007; Ahuja, 2009) are close to the ethane value (see Table 1). We implement a numerical calculation for the dynamic composition evolution of liquid mixtures using discrete timesteps. At each time t, the saturation mole fraction $X_{i,\mathrm{sat}}$ of each dissolved solid species i is computed via

$$\ln \Gamma_i X_{i,\mathrm{sat}} = -\frac{\Delta H_{i,\mathrm{m}}}{R T_{i,\mathrm{m}}} \left(\frac{T_{i,\mathrm{m}}}{T} - 1 \right) \tag{1}$$

This relation can be found, for instance, in the Section 8-16 of the textbook by Poling et al. (2007) (hereafter POL07). The physical significance of Equation (1) is the existence of a thermodynamic equilibrium between the considered precipitated solid i and the liquid solution. The enthalpy of melting is denoted $\Delta H_{i,\mathrm{m}}$, whereas T and $T_{i,\mathrm{m}}$ are respectively the current temperature of the lake and the melting temperature of molecule i; R is the constant of ideal gases and Γ_i is the activity coefficient. Although Equation (1) has previously been used in several published works (Dubouloz et al., 1989, hereafter D89, and also C09, C10 and C12), we recall that it is approximate and its validity will be discussed in Section 4.

As the thermodynamic computations in the frame of the regular solution theory are uncertain (see C12) due to the lack of knowledge of thermodynamic data, we have distinguished two cases: the approximation of the ideal solution for which all the Γ_i's are equal to unity, and the non-ideal regular solution. In the case of an ideal solution, the molecules of the same species and those of different species interact with same intensity. For a non-ideal solution model, the Γ_i's are computed in the frame of regular solution theory (see D89, C09, POL07) in which the intermolecular interactions of involved species are such that the resulting entropy of mixing is equal to that of an ideal solution with the same composition: zero excess entropy, with the volume of mixing at zero. However in contrast with ideal solutions, regular solutions have mixing enthalpy with nonzero values. The regular-solution theory provides a good and useful semiquantitative representation of real

behavior for solution containing nonpolar components as is the case of the mixtures under study in this work and the results based on this theory are in general considerably improved over those calculated by Raoult's law. In the context of the mixtures studied here it is expected that even though results may not possess extreme accuracy they are also hardly ever very bad, providing a valuable guide for future work. We emphasize that the Γ_i's are functions of X_i's, a fact which leads to numerical complications. The temperature T of the liquid remains unchanged during the whole evaporation process. Note, by the way, that for the temperatures relevant (see Table 1 for melting temperatures values) in our context, the right-hand side of Equation (1) is negative, leading to mole fractions lower than the unity, at least in the case of an ideal solution.

Table 1: Solids assumed to be dissolved in the lake and some of their properties. The Hildebrand's solubity parameter δ has to be compared to the value for methane and ethane at the same temperature (i.e. 90 K), which are respectively 1.52×10^4 $(\mathrm{J\,m^{-3}})^{1/2}$ and 2.19×10^4 $(\mathrm{J\,m^{-3}})^{1/2}$. For comparison purposes, for H_2O $\delta \sim 5 \times 10^4$ $(\mathrm{J\,m^{-3}})^{1/2}$.

Species	Precipitation rate	δ	Melting temperature	Enthalpy of melting
	$\mathrm{molecules\,m^{-2}\,s^{-1}}$	10^4 $(\mathrm{J\,m^{-3}})^{1/2}$	(K)	$(\mathrm{kJ\,mol^{-1}})$
HCN	$1.3 \times 10^{8(a)}$	2.99	260.0	8.406
C_4H_{10}	$5.4 \times 10^{7(a)}$	1.91	136.0	4.661
C_2H_2	$5.1 \times 10^{7(a)}$	2.28	192.4	4.105
CH_3CN	$4.4 \times 10^{6(a)}$	2.92	229.3	6.887
CO_2	$1.3 \times 10^{6(a)}$	1.98	216.6	9.020
C_6H_6	$1.0 \times 10^{6(b)}$	2.48	279.1	9.300

$^{(a)}$Lavvas et al. (2008a,b); $^{(b)}$Vuitton et al. (2008).

The equilibrium solid-solution written as Equation (1) must be complemented by the Principle of Matter Conservation. If we denote the total number of moles of all species at time t in the liquid by $N(t)$; at time $t + \mathrm{d}t$, one can write for a lake with surface area S

$$\begin{aligned} N(t+\mathrm{d}t) = N(t) \quad &- \quad F_{\mathrm{CH_4}} \times S \times \mathrm{d}t - F_{\mathrm{C_2H_6}} \times S \times \mathrm{d}t - F_{\mathrm{N_2}} \times S \times \mathrm{d}t \\ &- \quad \textstyle\sum_{i,\mathrm{sat},t+\mathrm{d}t} (X_i(t)\, N(t) - X_{i,\mathrm{sat}}^{\mathrm{ideal}} N(t+\mathrm{d}t)) \end{aligned} \tag{2}$$

where $F_{\mathrm{CH_4}}$, $F_{\mathrm{C_2H_6}}$ and $F_{\mathrm{N_2}}$ are the assumed respective evaporation rates

(in mole $\mathrm{m}^{-2}\,\mathrm{s}^{-1}$) of CH_4, C_2H_6 and N_2. The terms containing the F_i's represent the evaporation while the sum, which refers to species reaching the saturation at $t + \mathrm{d}t$, corresponds to matter that precipitates and deposits on the lake floor.

The number of mole of species i available in the volume $S \times H$ of lake, at time t, is denoted by $n_i(t)$. Thus we arrive at the simple relation $n_i(t) = X_i N(t)$. Our algorithm consists of several steps. For the first one, we compute $N^{(0)}(t + \mathrm{d}t)$. This is an estimation of the total number of moles (in volume $S \times H$ of lake) remaining after the time step $\mathrm{d}t$ during which only evaporation of methane, ethane and nitrogen is taken into account:

$$N^{(0)}(t + \mathrm{d}t) = N(t) - (F_{\mathrm{CH_4}} + F_{\mathrm{C_2H_6}} + F_{\mathrm{N_2}}) \times S \times \mathrm{d}t \quad . \tag{3}$$

From this, we can infer the corresponding mole fraction

$$X_i^{(0)} = \frac{n_i(t + \mathrm{d}t)}{N^{(0)}(t + \mathrm{d}t)} \tag{4}$$

with $n_i(t+\mathrm{d}t) = n_i(t)$ for all species except those belonging to the solvent. If, as a first attempt, we work in the frame of the ideal solution theory, then we have to compare the $X_i^{(0)}$'s to the mole fractions at saturation (for an ideal solution) $X_{i,\mathrm{sat}}^{\mathrm{ideal}}$. The molecules for which the criterion is fulfilled are presumed to precipitate. Their abundances are fixed to the saturation value

$$X_i(t + \mathrm{d}t) = X_{i,\mathrm{sat}}^{\mathrm{ideal}} \text{ (only species that saturate)} \quad , \tag{5}$$

and the total number of moles at $t+\mathrm{d}t$ in the volume $S \times H$ is recomputed to be

$$N(t+\mathrm{d}t) = \frac{\left[1 - \sum_{\mathrm{sat}} X_{i,\mathrm{sat}}\right] N(t) - (F_{\mathrm{CH_4}} + F_{\mathrm{C_2H_6}} + F_{\mathrm{N_2}}) \times S \times \mathrm{d}t}{1 - \sum_{\mathrm{sat}} X_{i,\mathrm{sat}}^{\mathrm{ideal}}} \quad . \tag{6}$$

Finally, the abundances at $t + \mathrm{d}t$ of species that do not saturate can be easily derived

$$X_i(t + \mathrm{d}t) = \frac{n_i(t)}{N(t + \mathrm{d}t)} \tag{7}$$

For a given species i that saturates, the rate of evaporite formation is then given by

$$F_i^{\rm evap}(t+{\rm d}t) = \frac{X_i(t)\,N(t) - X_{i,{\rm sat}}^{\rm ideal}\,N(t+{\rm d}t)}{S\times{\rm d}t} \quad . \tag{8}$$

The chemical composition of the formed evaporite at time $t+{\rm d}t$ is given by

$$X_i^{\rm evap}(t+{\rm d}t) = \frac{F_i^{\rm evap}(t+{\rm d}t)}{\sum\limits_{j,{\rm sat}} F_j^{\rm evap}(t+{\rm d}t)} \quad . \tag{9}$$

When the solution is considered as a "real" solution, i.e. the activity coefficients are not taken to be equal to the unity and depend on the mole fractions, then

$$\Gamma_i(t+{\rm d}t) = \Gamma_i(X_1(t+{\rm d}t), X_2(t+{\rm d}t), ...) \quad . \tag{10}$$

The scheme allowing the computation of evaporite composition when the solution is non-ideal is rather similar to that of the case of an ideal solution. However, there are some differences: the total number of moles $N(t+{\rm d}t)$ can no longer be computed with Eq. 6. Instead, if $N_{\rm sat}$ is the number of species saturating at $t+{\rm d}t$, then we solve the system of $(N_{\rm sat}+1)$ equations composed of Equation (2) and the $N_{\rm sat}$ equations similar to Equation (1). The unknowns are $N(t+{\rm d}t)$ and the $N_{\rm sat}$ mole fractions at saturation $X_{k,{\rm sat}}^{\rm non-ideal}$. The resolution of that non-linear system is performed using a multi-dimensional Newton-Raphson's method (see Press et al., 1992).

Several authors (Mitri et al., 2007; Tokano, 2005, 2009) have studied the dynamics of Titan's lakes. They have used the bulk aerodynamical model, introduced for Earth's climate model by Fairall et al. (1996). In this model the evaporation rate is given by

$$E = \rho_{\rm air}\,K\,(q^*-q)\,u_r \tag{11}$$

where E is expressed in $\mathrm{kg\,m^{-2}\,s^{-1}}$, $\rho_{\rm air}$ as the density of the air, K is a transport coefficient (a purely aerodynamic quantity), q^* and q are saturation specific humidity and specific humidity respectively, and u_r is the horizontal component of the averaged wind speed relative to the surface at a given height z_r. As we can see, the rate E depends on q and u_r, quantities that are supposed to undergo substantial

variations during a Titan's year. Thus the rate E is expected to experience significant variations during Titan's seasonal cycle. To obviate this

problem we have chosen to use two definitions of time and two time-scales, respectively corresponding to the evaporation of CH_4 and the evaporation of C_2H_6. Methane is known to be much more volatile than ethane. An order of magnitude of the ratio $\alpha_{\rm evap} = F_{C_2H_6}/F_{CH_4}$ can be evaluated thanks to the Hertz-Knudsen (see Ward and Fang, 1999, and references therein): one finds that $\alpha_{\rm evap} \sim 10^{-4}$ for a temperature $T \simeq 90$ K. In our model we fixed $\alpha_{\rm evap}$ to this value. The evaporation rate of nitrogen is scaled to the C_2H_6 one, in order to insure a N_2 content in the liquid preventing it from freezing (see Mitri et al., 2007). Therefore, all the CH_4 content evaporates on a short time-scale τ_{CH_4} during which the time t_{CH_4} is defined so that the evaporation rate F_{CH_4} is constant. We emphasize that this operation is equivalent to an implicit non-linear re-scaling of time. A similar definition is adopted for $t_{C_2H_6}$, the "variable time" valid during ethane evaporation, as $F_{CH_4} \gg F_{C_2H_6}$, the quantity of ethane escaping the lake during methane evaporation, is negligible. This way, all the details of the possible events (*e.g.*, low or high humidity, strong winds) that could affect the evaporation rates can be ignored.

3. Evaporites Upper Layer Composition Calculation

First we build plausible chemical compositions relevant for a lake before its evaporation. Previous calculations made at thermodynamic equilibrium (D89, C09) correspond to an averaged composition in time and space. Atmospheric precipitation rates are likely to undergo substantial secular variations — this is supported by some *Cassini* observations (see for instance Turtle et al., 2011a). In addition, the flux of hydrocarbons falling from the atmosphere likely varies significantly from one location to another: in the equatorial regions the presence of the dune fields indicates an arid climate while lakes, evidences for a wet weather, are located in the polar regions. These tendencies are confirmed by Global Circulation Models (see for instance Figure 4 of C12 based on Crespin et al., 2008). Thus we have considered methane-poor and -rich solvents, always containing a few percent of N_2. Concerning the solids possibly in solution, we used precipitation rates derived from 1D photochemical models by Lavvas et al. (2008a,b) and Vuitton et al. (2008)— the precipitation rates are recalled in Table 1. We stress that these rates have to be taken with caution because of the lack of micro-physics in the models. A compound that meets an altitude where the temperature equals its condensation temperature rains out. In addition, 3D physical processes (mainly transport) are ignored, although they can affect significantly the

amounts of solid hydrocarbons reaching the surface at a given place at a particular time. Two possibilities have been studied.

- In Type 1 solids mixture, where the abundances of these solids have been scaled to atmospheric precipitation rates, the most abundant species (*i.e.*, HCN) has its mole fraction set to its value at saturation (ideal solution case). This way, the precipitation (*i.e.*, saturation) of solids in solution in the liquid begins at the initial time. An assumed initial value below the saturation one, only delaying the starting time of precipitation, keeps the final composition of the upper layer of evaporites unchanged.

- Type 2 solids mixture, in order to appreciate the effect of evaporation/solids evaporites deposition, we constructed also initial mixtures with uniform abundances, and starting values fixed to the smallest mole fraction at saturation (i.e. that relative to C_6H_6). At the evaporation initial time, one species begins to precipitate (i.e. C_6H_6); the others saturate latter.

In Table 2, results relevant for an ideal solution have been gathered. Two initial mixtures have been considered — both ethane rich ($\sim 89\%$ of C_2H_6 when evaporation begins) with $\sim 1\%$ of nitrogen to ensure the liquid physical state. This abundance of N_2 is typical of what has been inferred by computations at equilibrium in previous works. While $X_{\rm liq}^{\rm ini}$ quantifies the initial chemical composition of the solution, $X_{\rm sol}^{\rm ini}$ represents the abundances of solutes regarded as a single set: $\sum X_{\rm sol}^{\rm ini} = 1$. The $X_{\rm evap}^{\rm fin}$'s are the mole fractions of compounds finally deposited in the evaporites upper layer. The parameter of enrichment Δ measures the relative enrichment/empoverishment of a given species in the surface evaporites, as compared to the initial composition of solids in solution.

As can be noticed in Table 2, the only species undergoing an enrichment in the surface evaporites layer, compared to abundances initially taken into account for the dissolved solids, are butane (C_4H_{10}) and acetylene (C_2H_2). This behavior can be explained by their high solubilities (i.e. high $X_{i,\rm sat}$'s). The higher $X_{i,\rm sat}$ is, the greater the quantity of dissolved material is. Consequently the saturation occurs later during the evaporation process. If we compare $X_{\rm fin}^{\rm evap}$ obtained for type 1 and type 2 mixtures of solids, we see that evaporite composition (perhaps unsurprisingly) depends on the initial abundances of solutes. Our simulation clearly shows, within the framework of our

Table 2: Computed chemical composition ($X^{\rm fin}_{\rm evap}$) of upper layer Titan's lakes drybeds evaporites, in the ideal solution hypothesis. Two types of dissolved solids composition have been considered (see text for explanation). $X_{i,\rm sat}$ is the mole fraction at saturation, $X_{i,\rm liq}$ represents the initial composition of the liquid and $X_{i,\rm sol}$ represents the initial abundances of dissolved solids. The Δ's show enrichment/empoverishment of the resulting upper layer of the evaporite deposit. The assumed temperature is $T = 90$ K. The notation $x.y(-n) = x.y \times 10^{-n}$ has been used. One can notice that ideal solubility of CO_2 is comparable to the values reported by Preston and Prausnitz (1970) and Preston et al. (1971) for somewhat higher temperatures around 130-140 K.

Ideal solution					
Species	$X_{i,\rm sat}$ (ideal)	Mixture type 1			
		$X^{\rm ini}_{\rm liq}$	$X^{\rm ini}_{\rm sol}$	$X^{\rm fin}_{\rm evap}$	Δ
CH_4	–	10.018%	–	–	–
C_2H_6	–	88.804%	–	–	–
N_2	–	1.002%	–	–	–
HCN	6.46 (−4)	6.46 (−4)	3.65 (−1)	3.82 (−3)	-99 %
C_4H_{10}	1.22 (−1)	5.93 (−4)	3.35 (−1)	6.48 (−1)	+94 %
C_2H_2	5.40 (−2)	3.62 (−4)	2.05 (−1)	3.20 (−1)	+56 %
CH_3CN	3.73 (−3)	5.42 (−5)	3.06 (−2)	2.21 (−2)	-28 %
CO_2	8.72 (−4)	3.43 (−5)	1.94 (−2)	5.16 (−3)	-73 %
C_6H_6	2.20 (−4)	8.06 (−5)	4.55 (−2)	1.31 (−3)	-97 %
		Mixture type 2			
		$X^{\rm ini}_{\rm liq}$	$X^{\rm ini}_{\rm sol}$	$X^{\rm fin}_{\rm evap}$	Δ
CH_4	–	10.013%	–	–	–
C_2H_6	–	88.853%	–	–	–
N_2	–	1.001%	–	–	–
HCN	6.46 (−4)	2.20 (−4)	1.67 (−1)	6.86 (−3)	-96 %
C_4H_{10}	1.22 (−1)	2.20 (−4)	1.67 (−1)	4.71 (−1)	+183 %
C_2H_2	5.40 (−2)	2.20 (−4)	1.67 (−1)	4.71 (−1)	+183 %
CH_3CN	3.73 (−3)	2.20 (−4)	1.67 (−1)	3.96 (−2)	-76 %
CO_2	8.72 (−4)	2.20 (−4)	1.67 (−1)	9.26 (−3)	-94 %
C_6H_6	2.20 (−4)	2.20 (−4)	1.67 (−1)	2.34 (−3)	-99 %

current assumptions, that dissolution in methane/ethane solution, followed by evaporation of the solvent, yields surface evaporite compositions with high abundances of the most soluble species.

Table 3: Type 1 mixtures in the case of a non-ideal solution. A methane poor and a methane rich case are considered.

Non-ideal solution				
Species	Mixture type 1, methane poor			
	$X^{\rm ini}_{\rm liq}$	$X^{\rm ini}_{\rm sol}$	$X^{\rm fin}_{\rm evap}$	Δ
CH_4	10.018%	–	–	–
C_2H_6	88.804%	–	–	–
N_2	1.002%	–	–	–
HCN	$6.46\,(-4)$	$3.65\,(-1)$	$1.52\,(-4)$	-100 %
C_4H_{10}	$5.93\,(-4)$	$3.35\,(-1)$	$5.72\,(-1)$	+71 %
C_2H_2	$3.62\,(-4)$	$2.05\,(-1)$	$4.20\,(-1)$	+105 %
CH_3CN	$5.42\,(-5)$	$3.06\,(-2)$	$7.14\,(-4)$	-98 %
CO_2	$3.43\,(-5)$	$1.94\,(-2)$	$6.53\,(-3)$	-66 %
C_6H_6	$8.06\,(-5)$	$4.55\,(-2)$	$6.82\,(-4)$	-99 %
	Mixture type 1, methane rich			
	$X^{\rm ini}_{\rm liq}$	$X^{\rm ini}_{\rm sol}$	$X^{\rm fin}_{\rm evap}$	Δ
CH_4	90.160 %	–	–	–
C_2H_6	8.662 %	–	–	–
N_2	1.002 %	–	–	–
HCN	$6.46\,(-4)$	$3.65\,(-1)$	$6.92\,(-5)$	-100 %
C_4H_{10}	$5.93\,(-4)$	$3.35\,(-1)$	$6.69\,(-1)$	+100 %
C_2H_2	$3.62\,(-4)$	$2.05\,(-1)$	$3.24\,(-1)$	+58 %
CH_3CN	$5.42\,(-5)$	$3.06\,(-2)$	$2.94\,(-4)$	-99 %
CO_2	$3.43\,(-5)$	$1.94\,(-2)$	$6.03\,(-3)$	-69 %
C_6H_6	$8.06\,(-5)$	$4.55\,(-2)$	$3.65\,(-4)$	-99 %

We stress that an identical value of the enrichment Δ is the consequence of a saturation of solutes that occurs at the very end of the evaporation. Of course, a solvent of a different composition (*e.g.*, a methane rich one) leads strictly to the same result because here we are making the calculations by adopting the ideal solution hypothesis.

Table 4: Type 2 mixtures in the case of a non-ideal solution. A methane poor and a methane rich case are considered.

Non-ideal solution				
Species	Mixture type 2 methane poor			
	$X_{\text{liq}}^{\text{ini}}$	$X_{\text{sol}}^{\text{ini}}$	$X_{\text{evap}}^{\text{fin}}$	Δ
CH_4	10.013 %	–	–	–
C_2H_6	88.853 %	–	–	–
N_2	1.001 %	–	–	–
HCN	$2.20\,(-4)$	$1.67\,(-1)$	$2.18\,(-4)$	-100 %
C_4H_{10}	$2.20\,(-4)$	$1.67\,(-1)$	$4.95\,(-1)$	+197 %
C_2H_2	$2.20\,(-4)$	$1.67\,(-1)$	$4.95\,(-1)$	+197 %
CH_3CN	$2.20\,(-4)$	$1.67\,(-1)$	$1.04\,(-3)$	-99 %
CO_2	$2.20\,(-4)$	$1.67\,(-1)$	$8.54\,(-3)$	-95 %
C_6H_6	$2.20\,(-4)$	$1.67\,(-1)$	$9.55\,(-4)$	-99 %
	Mixture type 2, methane rich			
	$X_{\text{liq}}^{\text{ini}}$	$X_{\text{sol}}^{\text{ini}}$	$X_{\text{evap}}^{\text{fin}}$	Δ
CH_4	90.119 %	–	–	–
C_2H_6	8.747 %	–	–	–
N_2	1.001 %	–	–	–
HCN	$2.20\,(-4)$	$1.67\,(-1)$	$6.97\,(-5)$	-100 %
C_4H_{10}	$2.20\,(-4)$	$1.67\,(-1)$	$6.68\,(-1)$	+301 %
C_2H_2	$2.20\,(-4)$	$1.67\,(-1)$	$3.25\,(-1)$	+ 95 %
CH_3CN	$2.20\,(-4)$	$1.67\,(-1)$	$2.97\,(-4)$	-100 %
CO_2	$2.20\,(-4)$	$1.67\,(-1)$	$6.03\,(-3)$	-96 %
C_6H_6	$2.20\,(-4)$	$1.67\,(-1)$	$3.67\,(-4)$	-100 %

The results of non-ideal simulations for the regular solution Γ_i's have been gathered in Table 3 and Table 4. Tables 3 and 4 are respectively devoted to dissolved solids mixture type 1 and type 2. For each of these types, cases of methane rich and poor solvent are considered. As can be noticed in Table 3 and Table 4, the general trend remains the same: butane and acetylene, if present in the initial mixture, are the dominant species in the upper evaporite layer. The difference between the results of methane rich and poor are explained by the non-ideality of the solution: in such a situation the molecules undergo interactions. In this way, solvents with different compositions are not equivalent.

Table 5: Influence of the initial nitrogen abundance on final evaporite layer composition. $T = 90$ K, non-ideal. Methane rich solvent ($X^{ini}_{\mathrm{CH_4}} \simeq 90\%$)

$X^{\mathrm{ini}}_{\mathrm{N_2}}$	0.5 %	1 %	3 %
	Δ	Δ	Δ
HCN	-99.9 %	-100.0 %	-100.0 %
C_4H_{10}	+270.5 %	+300.9 %	+377.5 %
C_2H_2	+125.0 %	+95.1 %	+19.1 %
CH_3CN	-99.7 %	-99.8 %	-100.0 %
CO_2	-96.2 %	-96.4 %	-96.7 %
C_6H_6	-99.7 %	-99.8 %	-100.0 %

The content of nitrogen is expected to vary slightly for different bodies of liquid. Hence we test for sensitivity of evaporite composition regarding the abundances of nitrogen in the solvent. Table 5 shows the enrichment parameter Δ for all solutes in three cases: $X^{\mathrm{ini}}_{\mathrm{N_2}} = 0.5\%$, 1% and 3%. All of these computations have been made for a methane rich solvent for a temperature of 90 K. Clearly, solvents with a high nitrogen abundance appear to favor C_4H_{10} as a main constituent of surface evaporites.

The temperature also influences the solubility of solids. For a range of temperatures (*i.e.*, 85 K, 90 K, and 95 K), the computed final compositions have been reported in Table 6. High values of temperature favors high-butane evaporite content, while acetylene is disfavored at high temperature. However the major tendency, the prominence of butane and acetylene, is robust. Finally, we stress that during all our calculations, for each time, we have checked that the density of species precipitating remained lower than the

Table 6: Influence of the temperature on final evaporite layer composition. The initial nitrogen mole fraction is fixed to $X_{N_2}^{ini} = 1\%$, the solution is a non-ideal one, and type 1 for the initial dissolved solids mixture has been considered.

Species	$T = 85$ K		$T = 90$ K		$T = 95$ K	
	methane poor solvent					
	X_{evap}^{fin}	Δ	X_{evap}^{fin}	Δ	X_{evap}^{fin}	Δ
HCN	$1.17\,(-4)$	-100	$1.52\,(-4)$	-100	$1.84\,(-4)$	-100
C_4H_{10}	$5.19\,(-1)$	+54.9	$5.72\,(-1)$	+70.7	$6.20\,(-1)$	+85.0
C_2H_2	$4.76\,(-1)$	+132.4	$4.20\,(-1)$	+105.3	$3.70\,(-1)$	+80.8
CH_3CN	$6.52\,(-4)$	-97.9	$7.14\,(-4)$	-97.7	$7.39\,(-4)$	-97.6
CO_2	$4.59\,(-3)$	-76.3	$6.53\,(-3)$	-66.3	$8.77\,(-3)$	-54.7
C_6H_6	$5.54\,(-4)$	-98.8	$6.82\,(-4)$	-98.5	$7.88\,(-4)$	-98.3
	methane rich solvent					
	X_{evap}^{fin}	Δ	X_{evap}^{fin}	Δ	X_{evap}^{fin}	Δ
HCN	$5.18\,(-5)$	-100	$6.92\,(-5)$	-100	$8.76\,(-5)$	-100
C_4H_{10}	$6.31\,(-1)$	+88.3	$6.69\,(-1)$	+99.8	$7.01\,(-1)$	+109.4
C_2H_2	$3.65\,(-1)$	+78.1	$3.24\,(-1)$	+58.4	$2.90\,(-1)$	+41.6
CH_3CN	$2.62\,(-4)$	-99.2	$2.94\,(-4)$	-99.0	$3.17\,(-4)$	-99.0
CO_2	$4.29\,(-3)$	-77.9	$6.03\,(-3)$	-68.9	$8.07\,(-3)$	-58.3
C_6H_6	$2.96\,(-4)$	-99.4	$3.65\,(-4)$	-99.2	$4.28\,(-4)$	-99.1

liquid solution value. Then, according to the simulations performed in this work, the organic precipitated solids would never float at the surface of the Titan's lakes (at least not without unusual circumstances such as those suggested by Hofgartner and Lunine, 2013).

4. Discussion and Conclusion

As it has been shown in the previous section, the composition obtained for the superficial layer of evaporite is the result of the influence of two main factors: (1) the initial composition of dissolved solids, and (2) the mole fraction at saturation values of the solids, provided by Equation (1). For a given initial composition, species with the highest $X_{i,\mathrm{sat}}$ (*i.e.*, the lowest energy of cohesion) remain dissolved for a longer time in the solvent during the evaporation and finally become the major constituents of the last layer of deposits. The value of the melting temperature T_m and enthalpy of melting determine the concentration at saturation. We furthermore emphasize that, due to the special non-linear scale of time used in this work, the depth of different layers of evaporite cannot be computed. In a same way, the composition of possible evaporite annuli around a lake (see for instance Hayes et al., 2010) could not be estimated. For a given initial composition of solids in solution, we can only compute the composition of the external surface of the evaporite deposit.

The behavior of those solid species that are not taken into consideration in this work could be estimated if their enthalpy of melting were known. For instance, laboratory experiments suggest that HC_3N could be an evaporite candidate in lake drybeds (Clark et al., 2010). In their Appendix II, Sagan and Thompson (1984) published a list of species with their estimated or estimated enthalpies of melting. HC_3N belongs to this list, these authors have found $\Delta H_\mathrm{m}(HC_3N) = 40\,\mathrm{cal\,g^{-1}}$, corresponding to $8.5\,\mathrm{kJ\,mol^{-1}}$. This value is a factor of 2 larger than enthalpies of melting for C_4H_{10} and C_2H_2. Coupled to an estimation of the temperature of melting of this molecule ~ 235 K (~ 235 K, obtained using a "group contribution" method, see Poling et al., 2007), one can derive that $X^{\mathrm{ideal}}_{\mathrm{sat},HC_3N} \simeq 10^{-3}$. Consequently, HC_3N should have a behavior ressembling that of CH_3CN. Thus, even if HC_3N has a precipitation rate larger than the acetylene rate, after a dissolution/evaporation process C_2H_2 should remain a dominant species in the final deposits layer.

Although the composition of tholins has not been directly measured, Quirico et al. (2008) identified in their experiments that molecules derived from hydrazine $R_1R_2N\text{-}NH_2$ as a possible constituent of Titan's atmosphere tholins. Taking the most simple molecules of that family: $CH_3CH_3N\text{-}NH_2$, one can estimate the value of the enthalpy ΔH_m thanks to a "group contribution" method (see Poling et al., 2007). We found $\Delta H_\mathrm{m} \simeq 9.15\ \mathrm{kJ\,mol^{-1}}$ and $T_\mathrm{m} \simeq 228$ K (for methylhydrazine Aston et al., 1951, found $\Delta H_\mathrm{m} \sim 10.42\ \mathrm{kJ\,mol^{-1}}$ and $T_\mathrm{m} \simeq 220.8$ K), yielding $X_\mathrm{sat}^\mathrm{ideal}(CH_3CH_3N\text{-}NH_2) \simeq 6 \times 10^{-4}$ — a value much smaller than the butane or acetylene ones.

However, hydrazine derivatives probably belong to tholins but are probably not representative of the whole. We recall that experiments and theoretical works made in the past have shown the poor solubility of tholins in non-polar solvents (McKay, 1996; Raulin, 1987). In a general manner, we can notice that ΔH_m increases when the number of $\text{-}CH_3$ get larger, suggesting that molecules with long carbon chains would be easily buried under layers rich in C_4H_{10} and C_2H_2.

The precipitation of solids previously dissolved in ternary solvent CH_4-C_2H_6-N_2 implies heterogeneous nucleation, which occurs much more often than homogeneous nucleation in the real world. Nucleation that forms at preferential sites such as phase boundaries or impurities like dust requires less energy than homogeneous nucleation (see for instance Vehkamäki, 2006). Depending on the initial turbidity of the lake, which might possibly caused by sediments produced during drainage and/or organic aggregates fallen from the atmosphere, the deposition of evaporites could begin either on the lake floor alone or simultaneously on this floor and on the particules contributing to the initial turbidity. Moreover, the formation of evaporite has to occur on a time-scale significantly shorter than that of evaporation, otherwise the concept used for our non-linear evaporation time-scale would no longer be relevant. In other words, solution cannot remain "supersaturated" for a long time.

If the formation of evaporite on the lake bed is the dominant effect, then a model based on solubility is fully valid. Otherwise, if the evaporites form preferentially on possible turbidity particulates, then the scenario of lake drybed deposition formation could be very different as it could involve transport processes like convection and sedimentation. Unfortunately, given that the turbidity of Titan's lakes is unknown, one can only guess that it should be very variable from one lake to another, being a function of the exact history

of the lake (drainage, occurence of a recent methane rainfall, etc.). Insight into turbidity and its time-variability could be acquired by direct measurements from a floating capsule, as were proposed by the Titan Mare Explorer (TiME) (Lorenz et al., 2012).

Finally, the validity of the theory presented in this article has to be considered. As indicated in Section 2, the Equation (1) is an approximation, and the rigourous formula is (see or instance Hojjati and Rohani, 2006)

$$\ln \Gamma_i X_{i,\mathrm{sat}} = -\frac{\Delta H_{i,\mathrm{m}}}{RT_{i,\mathrm{m}}} \left(\frac{T_{i,\mathrm{m}}}{T} - 1 \right) - \frac{1}{RT} \int_{T_m}^{T} \Delta c_p \, \mathrm{d}T + \frac{1}{R} \int_{T_m}^{T} \frac{\Delta c_p}{T} \, \mathrm{d}T \quad (12)$$

with

$$\Delta c_p = c_p(\text{subcooled liquid solute}) - c_p(\text{solid solute}) \quad (13)$$

(see p. 8.181 of POL07). The Equation (1) is a good approximation of Equation (12) when the contributions of the second and the third terms of the right-hand side are negligible, as is often the case as emphasized in the literature (see Poling et al., 2007; Hojjati and Rohani, 2006). This assumption has been made in previous work (D89, C09, C10 and C12). Unfortunately, reliable estimations of Δc_p are not feasible with available data. The Dulong & Petit law is probably not adequate for c_p(solid solute) at such a low temperature ($\sim$ 90 K), in which case the use of more sophisticated formulation like Debye's model (Kittel et al., 2004) would be required. However a Debye formulation is not currently applicable due to the lack of data. Besides this, Rùzicka & Domalski's method for determining c_p (subcooled liquid solute) (see p. 6.19 of POL07) is not relevant as interpolation expressions have a domain of validity limited to temperatures ranging from the melting point to the boiling point. For our purposes, the relevant temperature is well below the typical boiling point temperatures of considered species (see table 1).

However, even if the second and the third terms of the right-hand side of Equation 12 have significant values compared to that of the first term, the process of solid dissolution and formation of an evaporite deposit is certainly not neutral concerning the chemical composition of the solids visible at the surface. If quantitative determinations could be changed by the contribution of those two additional terms compared to present results, then the scenario of dissolution of solids coming directly from the atmospheric precipitation or

surrounding terrains (washing and deposition in lakebeds) after an evaporation episode would be robust. Such a scenario provides an explanation for the strong correlation of 5-μm brightness observations with morphologic dry beds RADAR detections. Several authors (McKay and Smith, 2005; Schulze-Makuch and Grinspoon, 2005; Lunine, 2010) have proposed the hypothesis of an exotic form of life based on a metabolism involving a chemical reaction between surface acetylene and atmospheric hydrogen. We underline that in such a context, our results have to be handled with extreme caution.

As previously suggested by C12 for the composition of lakes, more reliable predictions of Titan's lakes' drybeds could be made using in vitro simulations. But that would require a huge experimental effort that couples the evaporation of a ternary mixture and dissolution of solids hydrocarbons and nitriles in a cryogenic range of temperature. Already, Luspay-Kuti et al. (2012) have determined the evaporation rate of CH_4 and Malaska and Hodyss (2013) haved obtained promising preliminary results concerning the solubility of benzene.

In the recent past, an infrared VIMS observation (Stephan et al., 2010; Barnes et al., 2011b; Soderblom et al., 2012) has been explained by the occurrence of a probable specular reflection on a filled Titan's lake. A search for similar specular or near-specular reflections over dry beds could be of interest to constrain the nature of the evaporitic surface. A glint associated to an empty lake could be the signature of a smooth and thick evaporite layer, while no glint or a diffuse glint could help to constrain the evaporites' particle size distribution.

References

Ahuja, P., 2009. Chemical Engineering Thermodynamics. Prentice-Hall of India, New Dehli – 110001.

Aston, J., Finke, H., Janz, G., Russell, K., 1951. The Heat Capacity, Heats of Fusion and Vaporization, Vapor Pressures, Entropy and Thermodynamic Functions of Methylhydrazine. J. Am. Chem. Soc. 73, 1939.

Barnes, J. W., Bow, J., Schwartz, J., Brown, R. H., Soderblom, J. M., Hayes, A. G., Vixie, G., Le Mouélic, S., Rodriguez, S., Sotin, C., Jaumann, R., Stephan, K., Soderblom, L. A., Clark, R. N., Buratti, B. J., Baines, K. H.,

Nicholson, P. D., Nov. 2011a. Organic sedimentary deposits in Titan's dry lakebeds: Probable evaporite. Icar 216, 136–140.

Barnes, J. W., Brown, R. H., Soderblom, J. M., Soderblom, L. A., Jaumann, R., Jackson, B., Le Mouélic, S., Sotin, C., Buratti, B. J., Pitman, K. M., Baines, K. H., Clark, R. N., Nicholson, P. D., Turtle, E. P., Perry, J., May 2009. Shoreline features of Titan's Ontario Lacus from Cassini/VIMS observations. Icar 201, 217–225.

Barnes, J. W., Soderblom, J. M., Brown, R. H., Soderblom, L. A., Stephan, K., Jaumann, R., Mouélic, S. L., Rodriguez, S., Sotin, C., Buratti, B. J., Baines, K. H., Clark, R. N., Nicholson, P. D., Jan. 2011b. Wave constraints for Titan's Jingpo Lacus and Kraken Mare from VIMS specular reflection lightcurves. Icarus 211, 722–731.

Clark, R. N., Curchin, J. M., Barnes, J. W., Jaumann, R., Soderblom, L., Cruikshank, D. P., Brown, R. H., Rodriguez, S., Lunine, J., Stephan, K., Hoefen, T. M., Le Mouélic, S., Sotin, C., Baines, K. H., Buratti, B. J., Nicholson, P. D., Oct. 2010. Detection and mapping of hydrocarbon deposits on Titan. Journal of Geophysical Research (Planets) 115, 10005.

Cordier, D., Mousis, O., Lunine, J. I., Lavvas, P., Vuitton, V., Dec. 2009. An Estimate of the Chemical Composition of Titan's Lakes. ApJL 707, L128–L131.

Cordier, D., Mousis, O., Lunine, J. I., Lavvas, P., Vuitton, V., May 2013. Erratum: "An Estimate of the Chemical Composition of Titan's Lakes" ¡A href="/abs/2009ApJL..707L.128C"¿(2009, ApJL, 707, L128)¡/A¿. ApJL 768, L23.

Cordier, D., Mousis, O., Lunine, J. I., Lebonnois, S., Lavvas, P., Lobo, L. Q., Ferreira, A. G. M., Oct. 2010. About the Possible Role of Hydrocarbon Lakes in the Origin of Titan's Noble Gas Atmospheric Depletion. ApJL 721, L117–L120.

Cordier, D., Mousis, O., Lunine, J. I., Lebonnois, S., Rannou, P., Lavvas, P., Lobo, L. Q., Ferreira, A. G. M., Feb. 2012. Titan's lakes chemical composition: Sources of uncertainties and variability. PSS 61, 99–107.

Cornet, T., Bourgeois, O., Le Mouélic, S., Rodriguez, S., Sotin, C., Barnes, J. W., Brown, R. H., Baines, K. H., Buratti, B. J., Clark, R. N., Nicholson,

P. D., Jul. 2012. Edge detection applied to Cassini images reveals no measurable displacement of Ontario Lacus' margin between 2005 and 2010. Journal of Geophysical Research (Planets) 117, 7005.

Crespin, A., Lebonnois, S., Vinatier, S., Bézard, B., Coustenis, A., Teanby, N. A., Achterberg, R. K., Rannou, P., Hourdin, F., Oct. 2008. Diagnostics of Titan's stratospheric dynamics using Cassini/CIRS data and the 2-dimensional IPSL circulation model. Icarus 197, 556–571.

Dubouloz, N., Raulin, F., Lellouch, E., Gautier, D., Nov. 1989. Titan's hypothesized ocean properties - The influence of surface temperature and atmospheric composition uncertainties. Icarus 82, 81–96.

Fairall, C. W., Bradley, E. F., Rogers, D. P., Edson, J. B., Young, G. S., 1996. Bulk parameterization of air-sea fluxes for tropical ocean-global atmosphere coupled-ocean atmosphere response experiment. JGR 101 (C2), 3747 – 3764.

Hayes, A. G., Aharonson, O., Lunine, J. I., Kirk, R. L., Zebker, H. A., Wye, L. C., Lorenz, R. D., Turtle, E. P., Paillou, P., Mitri, G., Wall, S. D., Stofan, E. R., Mitchell, K. L., Elachi, C., Jan. 2011. Transient surface liquid in Titan's polar regions from Cassini. Icar 211, 655–671.

Hayes, A. G., Wolf, A. S., Aharonson, O., Zebker, H., Lorenz, R., Kirk, R. L., Paillou, P., Lunine, J., Wye, L., Callahan, P., Wall, S., Elachi, C., Sep. 2010. Bathymetry and absorptivity of Titan's Ontario Lacus. Journal of Geophysical Research (Planets) 115, 9009–+.

Hofgartner, J. D., Lunine, J. I., Mar. 2013. Does ice float in Titan's lakes and seas? Icarus 223, 628–631.

Hojjati, H., Rohani, S., 2006. Measurement and Prediction of Solubility of Paracetamol in Water – Isopropanol Solution. Part 2. Prediction. Organic Process Research & Development 10, 1110–1118.

Jennings, D. E., Flasar, F. M., Kunde, V. G., Samuelson, R. E., Pearl, J. C., Nixon, C. A., Carlson, R. C., Mamoutkine, A. A., Brasunas, J. C., Guandique, E., Achterberg, R. K., Bjoraker, G. L., Romani, P. N., Segura, M. E., Albright, S. A., Elliott, M. H., Tingley, J. S., Calcutt, S., Coustenis, A., Courtin, R., Feb. 2009. Titan's Surface Brightness Temperatures. ApJL 691, L103–L105.

Kittel, C., Zettl, A., McEuen, P., 2004. Introduction to Solid State Physics. John Wiley & Sons.

Lavvas, P. P., Coustenis, A., Vardavas, I. M., Jan. 2008a. Coupling photochemistry with haze formation in Titan's atmosphere, Part I: Model description. Planet. Space Sci. 56, 27–66.

Lavvas, P. P., Coustenis, A., Vardavas, I. M., Jan. 2008b. Coupling photochemistry with haze formation in Titan's atmosphere, Part II: Results and validation with Cassini/Huygens data. Planet. Space Sci. 56, 67–99.

Lorenz, R. D., Stofan, E., Lunine, J. I., Zarnecki, J. C., Harri, A.-M., Karkoschka, E., Newman, C. E., Bierhaus, E. B., Clark, B. C., Yelland, M., Leese, M. R., Boldt, J., Darlington, E., Neish, C. D., Sotzen, K., Arvelo, J., Rasbach, C., Kretsch, W., Strohbehn, K., Grey, M., Mann, J., Zimmerman, H., Reed, C., Oct. 2012. MP3 - A Meteorology and Physical Properties Package for Titan Air-Sea Studies. LPI Contributions 1683, 1072.

Lunine, J. I., May 1993a. Does Titan have an ocean? A review of current understanding of Titan's surface. RGe 31, 133–149.

Lunine, J. I., 1993b. Erratum: "Does Titan have an ocean? A review of current understanding of Titan's surface" [Rev. Geophys., 31, 133-149 (1993)]. RGe 31, 355–356.

Lunine, J. I., 2010. Titan and habitable planets around M-dwarfs. Faraday Discussions 147, 405.

Lunine, J. I., Stevenson, D. J., Yung, Y. L., Dec. 1983. Ethane ocean on Titan. Sci 222, 1229–+.

Luspay-Kuti, A., Chevrier, V. F., Wasiak, F. C., Roe, L. A. Welivitiya, W., Cornet, T. Singh, S. R. E. G., Oct. 2012. Experimental simulations of CH_4 evaporation on Titan. GRL 39, L23203.

Malaska, M., Hodyss, R., Mar. 2013. Laboratory Investigation of Benzene Dissolving in a Titan Lake. LPI Contributions 1719, 2744.

McKay, C. P., Aug. 1996. Elemental composition, solubility, and optical properties of Titan's organic haze. PSS 44, 741–747.

McKay, C. P., Smith, H. D., Nov. 2005. Possibilities for methanogenic life in liquid methane on the surface of Titan. Icarus 178, 274–276.

Mitri, G., Showman, A. P., Lunine, J. I., Lorenz, R. D., Feb. 2007. Hydrocarbon lakes on Titan. Icar 186, 385–394.

Poling, B. E., Prausnitz, J. M., O'Connell, J., 2007. The Properties of Gases and Liquids, 5th Edition. McGraw-Hill Professional, Englewood Cliffs.

Press, W., Teukolsky, S., Vetterling, W., Flannery, B., 1992. Numerical Recipes in Fortran 77. Cambridge University Press.

Preston, G. T., Funk, E. W., Prausnitz, J. M., 1971. Solubilities of Hydrocarbons and Carbon Dioxide in Liquid Methane and in Liquid Argon. The Journal of Physical Chemistry 75, 2345.

Preston, G. T., Prausnitz, J. M., 1970. Thermodynamics of Solid Solubility in Cryogenic Solvents. Ind. Eng. Chem. Process Des. Develop. 9, 264.

Quirico, E., Montagnac, G., Lees, V., McMillan, P. F., Szopa, C., Cernogora, G., Rouzaud, J.-N., Simon, P., Bernard, J.-M., Coll, P., Fray, N., Minard, R. D., Raulin, F., Reynard, B., Schmitt, B., Nov. 2008. New experimental constraints on the composition and structure of tholins. Icar 198, 218–231.

Raulin, F., 1987. Organic chemistry in the oceans of Titan. Advances in Space Research 7, 71–81.

Sagan, C., Dermott, S. F., Dec. 1982. The tide in the seas of Titan. Natur 300, 731–733.

Sagan, C., Thompson, W. R., Aug. 1984. Production and condensation of organic gases in the atmosphere of Titan. Icar 59, 133–161.

Schulze-Makuch, D., Grinspoon, D. H., 2005. Biologically Enhanced Energy and Carbon Cylcing on Titan? Astrobiology 5, 560.

Soderblom, J. M., Barnes, J. W., Soderblom, L. A., Brown, R. H., Griffith, C. A., Nicholson, P. D., Stephan, K., Jaumann, R., Sotin, C., Baines, K. H., Buratti, B. J., Clark, R. N., Aug. 2012. Modeling specular reflections from hydrocarbon lakes on Titan. Icar 220, 744–751.

Stephan, K., Jaumann, R., Brown, R. H., Soderblom, J. M., Soderblom, L. A., Barnes, J. W., Sotin, C., Griffith, C. A., Kirk, R. L., Baines, K. H., Buratti, B. J., Clark, R. N., Lytle, D. M., Nelson, R. M., Nicholson, P. D., Apr. 2010. Specular reflection on Titan: Liquids in Kraken Mare. GRL 37, 7104.

Stofan, E. R., Elachi, C., Lunine, J. I., Lorenz, R. D., Stiles, B., Mitchell, K. L., Ostro, S., Soderblom, L., Wood, C., Zebker, H., Wall, S., Janssen, M., Kirk, R., Lopes, R., Paganelli, F., Radebaugh, J., Wye, L., Anderson, Y., Allison, M., Boehmer, R., Callahan, P., Encrenaz, P., Flamini, E., Francescetti, G., Gim, Y., Hamilton, G., Hensley, S., Johnson, W. T. K., Kelleher, K., Muhleman, D., Paillou, P., Picardi, G., Posa, F., Roth, L., Seu, R., Shaffer, S., Vetrella, S., West, R., Jan. 2007. The lakes of Titan. Nature 445, 61–64.

Tokano, T., 2005. Thermal structure of putative hydrocarbon lakes on Titan. Advances in Space Research 36, 286–294.

Tokano, T., Mar. 2009. Limnological Structure of Titan's Hydrocarbon Lakes and Its Astrobiological Implication. ASTROBIOLOGY 9, 147–164.

Turtle, E. P., Perry, J. E., Hayes, A. G., Lorenz, R. D., Barnes, J. W., McEwen, A. S., West, R. A., Del Genio, A. D., Barbara, J. M., Lunine, J. I., Schaller, E. L., Ray, T. L., Lopes, R. M. C., Stofan, E. R., Mar. 2011a. Rapid and Extensive Surface Changes Near Titan's Equator: Evidence of April Showers. Sci 331, 1414–.

Turtle, E. P., Perry, J. E., Hayes, A. G., McEwen, A. S., Apr. 2011b. Shoreline retreat at Titan's Ontario Lacus and Arrakis Planitia from Cassini Imaging Science Subsystem observations. Icar 212, 957–959.

Vehkamäki, H., 2006. Classical Nucleation Theory in Multicomponent Systems. Springer, Berlin, Heidelberg.

Vinatier, S., Bézard, B., Nixon, C. A., Mamoutkine, A., Carlson, R. C., Jennings, D. E., Guandique, E. A., Teanby, N. A., Bjoraker, G. L., Michael Flasar, F., Kunde, V. G., Feb. 2010. Analysis of Cassini/CIRS limb spectra of Titan acquired during the nominal mission. I. Hydrocarbons, nitriles and CO_2 vertical mixing ratio profiles. Icar 205, 559–570.

Vuitton, V., Yelle, R. V., Cui, J., May 2008. Formation and distribution of benzene on Titan. Journal of Geophysical Research (Planets) 113, 5007–+.

Wall, S., Hayes, A., Bristow, C., Lorenz, R., Stofan, E., L. J., Le Gall, A., Janssen, M., Lopes, R., Wye, L., Soderblom, L., Paillou, P., Aharonson, O., Zebker, H., Farr, T., Mitri, R., Kirk, R., Mitchell, K., Notarnicola, C., Casarano, D., Ventura, B., 2010. Active shoreline of Ontario Lacus, Titan: A morphological study of the lake and its surroundings. Geophysical Research Letters 37, L05202.

Ward, C. A., Fang, G., 1999. Expression for predicting liquid evaporation flux: Statistical rate theory approach. Physical Review E 59, 429.

We acknowledge financial support from the Observatoire des Sciences de l'Univers THETA Franche-Comt-Bourgogne, France. We thank Sandrine Vinatier and Panayotis Lavvas for scientific discussion; and the anonymous Reviewers who improved the clarity of the paper with their remarks and comments. JWB is funded by the NASA CDAPS Program Grant #NNX12AC28G.